SLC7A5 regulates tryptophan uptake and PD-L1 expression levels via the kynurenine pathway in ovarian cancer

RUIBIN JIANG[1], BO JIN[2], YUTING SUN[1], ZHONGJIAN CHEN[1,3], DANYING WAN[1], JIANGUO FENG[1,3], LISHA YING[1], CHANJUAN PENG[1] and LINHUI GU[1,3]

[1]Experimental Research Center, Zhejiang Cancer Hospital, Hangzhou, Zhejiang 310022, P.R. China; [2]College of Life Science, Zhejiang Chinese Medical University, Hangzhou, Zhejiang 310053, P.R. China; [3]Zhejiang Key Laboratory of Diagnosis and Treatment Technology on Thoracic Oncology (Lung and Esophagus), Zhejiang Cancer Hospital, Hangzhou, Zhejiang 310022, P.R. China

Received July 15, 2023; Accepted September 17, 2024

DOI: 10.3892/ol.2024.14772

Abstract. Ovarian cancer is the third most common gynecological malignancy worldwide and the fifth leading cause of cancer-related death among women. This may be attributed to difficulties in diagnosing early-stage ovarian cancer, as it is typically asymptomatic until metastases, and due to the ineffective management of patients with late-stage ovarian cancer. The aim of the present study was to investigate potential therapeutic targets for the treatment of ovarian cancer. Bioinformatics techniques were used to analyze the expression levels of tryptophan (Trp) metabolism-related genes in tissue samples from patients with ovarian cancer. Additionally, western blots, clonogenic assays, immunohistochemical staining, chromatin immunoprecipitation-quantitative PCR, cell co-culture assays, a xenograft model and high-performance liquid chromatography-tandem mass spectrometry were performed to evaluate the antitumor effects of genes identified from the bioinformatics analysis. Increased expression levels of the amino acid transporter, solute carrier family 7 member 5 (SLC7A5), in tissue samples from patients with ovarian cancer was demonstrated. Inhibition of SLC7A5 reduced ovarian cancer cell proliferation through G_2/M cell cycle arrest and blocked intracellular aryl hydrocarbon receptor nucleus entry, which downregulated PD-L1 expression levels. Dysregulation of Trp metabolism in ovarian cancer tissue samples, as well as the upregulation of kynurenine expression levels in the plasma of patients with ovarian cancer, were demonstrated to be unfavorable prognostic factors for the progression-free survival of patients with ovarian cancer. The present study demonstrated that the dysregulation of Trp metabolism could potentially be used as a diagnostic biomarker for ovarian cancer, as well as the potential of targeting SLC7A5 for immunotherapeutic management of patients with ovarian cancer in the future.

Correspondence to: Professor Linhui Gu, Experimental Research Center, Zhejiang Cancer Hospital, 1 East Banshan Road, Gongshu, Hangzhou, Zhejiang 310022, P.R. China
E-mail: gulh@zjcc.org.cn

Key words: ovarian cancer, solute carrier family 7 member 5, tryptophan, kynurenine, aryl hydrocarbon receptor, programmed death-ligand 1

Introduction

Ovarian cancer is the third most common gynecological malignancy worldwide and the fifth leading cause of cancer-related death among women (1), with ~200,000 cases diagnosed annually worldwide (2). A large proportion of patients with ovarian cancer are diagnosed at late stages of the disease, due to the lack of symptoms during early stages of the disease. This is associated with a notable reduction in the 5-year survival rate, which decreases from 93.5% for patients with stage I cancer to <30% for patients with stage IV cancer (3,4). Current available treatments for ovarian cancer include surgery, chemotherapy and radiotherapy. However, these strategies have clinical limitations, including the late stage at the time of discovery, the loss of surgery opportunities and that chemotherapy can lead to drug resistance (5). Therefore, the discovery of new therapeutic targets in ovarian cancer is needed to improve the treatment outcomes for patients.

Previous studies have demonstrated that cancer cells can rewire their cellular metabolism to support the demands of tumorigenesis, cell growth and survival, cellular communication and cancer metastasis (6-9). The Warburg effect is a process of metabolic reprogramming in cancer cells, which describes the preference of cancer cells to metabolize glucose anaerobically instead of aerobically (10-15). Disorders relating to tryptophan (Trp) metabolism have gained interest as a potential therapeutic target in ovarian cancer. Previous studies have reported that Trp metabolism is overactive in a certain types of tumors, such as gliomas (16), liver cancer (17) and cervical cancer (18), which promotes a malignant phenotype and inhibition of tumor immunity. Trp is an essential amino acid and Trp metabolism can lead to the production of serotonin and metabolites through the kynurenine (Kyn) pathway (19). In the Kyn pathway, kynurenine is produced by tryptophan metabolism, which serves important roles in promoting the pathogenesis of cancer (20,21). Studies have demonstrated the impact of the Kyn pathway on the tumor microenvironment and its biological effects on tumor immunological responses (22,23), where

Kyn serves as a key functional molecule that can activate the signaling of ligand-activated transcription factor AHR and transduce tumor immune escape (24). By contrast, PD-L1 is an immune checkpoint that is expressed in cancer cells (25) and its expression is modulated by cytokines, including TNF-α, VEGF and IFN (26). Although PD-L1 blockade therapy has shown promise in clinical practice, the underlying mechanism of this is currently unclear. Therefore, the reduction of Kyn expression levels may be an important strategy for the treatment of ovarian cancer.

In vitro and *in vivo* assays were performed to investigate the role of amino acid transporters in ovarian cancer cells. In addition, the clinical samples were analyzed by metabonomics. The present study aimed to facilitate the discovery of novel therapeutic targets and treatment strategies for the treatment of ovarian cancer.

Materials and methods

Tissue and plasma samples. Ovarian tissue samples and plasma were obtained from a biorepository at the Zhejiang Cancer Hospital (Hangzhou, China) and the patients admitted from 1st January 2016 to 31st December 2017. Patients and healthy donors that were enrolled in the present study provided written informed consent. All patients received standard clinical treatment. Patients and healthy donors were aged between 19-89 years. The present study was performed retrospectively and was approved by the Ethics Committee of the Zhejiang Cancer Hospital (approval no. IRB-2021-315; Hangzhou, China).

Tissue and plasma samples were collected during surgery from patients that were diagnosed with either advanced serous ovarian cancer or benign cysts (tissue, Table I; plasma, Table II). Tissue samples were stored at -80˚C following sample collection. Plasma was immediately separated from blood samples after collection by centrifugation at 1,200 x g for 10 min at 4˚C, which was then aliquoted and stored at -80˚C. Patient-derived cells (PDCs) were obtained from a patient with ovarian cancer (female, 65 years old) during surgery in Zhejiang Cancer Hospital on 8th August 2017. These generation of these PDCs were described in our previous study (2) and approved by the Ethics Committee of the Zhejiang Cancer Hospital [approval no. (2015)-1-7; Hangzhou, China]. The expression levels of the genes identified in ovarian cancer classed according to tumor grade were analyzed using the University of ALabama at Birmingham CANcer data analysis Portal software (http://ualcan.path.uab.edu/index.html).

Cell lines and chemicals. The ovarian cancer cell lines SKOV3, ID8 and ES-2 (short tandem repeat profiling certified) were purchased from the American Type Culture Collection. The cells were cultured in an incubator at 37˚C and 5% CO_2. SKOV3 cells were cultured in MyCoy's 5A medium (Gibco; Thermo Fisher Scientific, Inc.) supplemented with 10% FBS (Gibco; Thermo Fisher Scientific, Inc.) and 1% penicillin-streptomycin (Beijing Solarbio Science & Technology Co., Ltd.). MyCoy's 5A medium without Trp (Wuhan Boster Biological Technology, Ltd.) was used to culture cells for Trp starvation experiments. ES-2 and ID8 cells were cultured in Roswell Park Memorial Institute 1640 medium (Gibco; Thermo Fisher Scientific, Inc.) supplemented with 10% FBS and 1% penicillin-streptomycin. All cell lines were tested using the Cell Culture Contamination Detection Kit (Thermo Fisher Scientific, Inc.) to ensure that the cells were negative for mycoplasma contamination.

L-Trp and L-Kyn were purchased from MedChem Express. BCH (TargetMol; cat. no. T11820; Shanghai Topscience Co., Ltd.) and JPH203 (TargetMol; cat. no. TQ0081; Shanghai Topscience Co., Ltd.) were purchased from TargetMol Chemicals Inc. ^{13}C-Trp was purchased from Sigma-Aldrich (Merck KGaA).

Cell transfections. Lentiviruses encoding the short hairpin (sh)RNA targeting human SLC7A5 and an shRNA scramble sequence (negative control) were purchased from OBiO Technology (Shanghai) Corp., (Table III). The lentivirus containing the mouse shSLC7A5 and shRNA scramble sequence (negative control) were purchased from Shanghai Genechem Co., Ltd. Briefly, the shRNA target human SLC7A5 was cloned into a pSLenti-U6-shRNA-CMV-EGFP-F2A-Puro-WPRE vector and the shRNA target mouse SLC7A5 was cloned into a hU6-MCS-CBh-gcGFP-IRES-puromycin vector, resulting in a lenti-shSLC7A5 construct for knockdown. The MOI used to infect SKOV3 and ID8 cells were 10, with a transduction duration of 24 h. After 24 h of transfection, the cells were washed with D-PBS and replaced with complete medium. During this period, cells were treated with 2 μg/ml puromycin for 5 days to establish stable knockdown cells, and then maintained in culture with 1 μg/ml puromycin. Detection of knockdown efficiency was determined by western blotting.

Tissue metabolic profiling. In total, tissue samples from 77 patients diagnosed with advanced serous ovarian cancer and 40 patients diagnosed with benign cysts were included in the present tissue-based metabolic profiling analysis. To process tissue samples, ~10 mg of frozen tissue was mixed with 400 μl of ice-cold methanol for 5 min. Each tissue sample was homogenized and centrifuged at 16,200 x g for 15 min at 4˚C. An aliquot of 200 μl of the supernatant was mixed with 200 μl of water and freeze-dried. Reconstruction was achieved using 80 μl 25% acetonitrile and mixing for 1 min. The sample was then centrifuged at 16,200 x g for 15 min at 4˚C and 10 μl of supernatant used for LC-MS analysis. The LC-MS conditions were similar to those previously described (27). In brief, an Ultimate 3000 Ultra-High-Performance LC System (Dionex; Thermo Fisher Scientific, Inc.) coupled to a Q Exactive Orbitrap mass spectrometer (Thermo Fisher Scientific, Inc.) was used for the analysis. The separation was conducted on an ACQUITY UPLC HSS T3 column (Waters Corporation) that had an internal diameter of 2.1x100.0 mm and particle size of 1.8 mm at 35˚C. The mobile phase consisted of acetonitrile (A) and water containing 0.1% formic acid (B), with a flow rate set at 0.3 ml/min. A gradient elution was employed, starting with 2% A from 0 to 1 min, followed by a gradient from 2 to 100% A from 1 to 10 min. This was held at 100% A for 3 min. Subsequently, the mobile phase was adjusted from 100 to 2% A from 13 to 13.1 min, and then maintained at 2% A from 13.1 to 16 min. The spray voltage values were set to 3.5 and 2.5 kV in positive and negative modes, respectively. The

Table I. Baseline characteristics of patient with tumors and benign cysts of included tissue samples.

A, Benign cases	
Characteristic	No. of patients, n
Age, years	
<60	25
≥60	15

B, Tumor cases	
Characteristic	No. of patients, n
Age, years	
<60	48
≥60	29
Menarche age, years	
<15	30
≥15	47
Menopause	
Yes	65
No	12
Histology	
Non-serous	3
Serous	74
Clinical stage	
I-II	4
III-IV	72
Missing	1
Alcohol consumption	
Yes	0
No	77
Smoking status	
Yes	0
No	77
Family history of ovarian cancer	
Yes	27
No	50

Table II. Baseline characteristics of the healthy patients and patients with cancer of included serum samples.

A, Healthy cases	
Characteristic	No. of patients, n
Age, years	
<60	44
≥60	10

B, Tumor cases	
Characteristic	No. of patients, n
Age, years	
<60	142
≥60	60
Menarche age, years	
<15	50
≥15	151
Missing	1
Menopause	
Yes	134
No	68
Histology	
Non-serous	50
Serous	152
Clinical stage	
I-II	21
III-IV	174
Missing	7
Alcohol consumption	
Yes	0
No	202
Smoking status	
Yes	0
No	202
Family history of ovarian cancer	
Yes	6
No	196

capillary temperatures were set to 320˚C for positive mode and 350˚C for negative mode. Sheath gas flow rates were adjusted to 35 and 40 Arb for positive and negative modes, respectively. The S-Lens RF level was maintained at 55 in both modes. Full mass scans were conducted across a range of m/z 70-1,000, with automatic gain control set to $3x10^6$ for both modes. For MS/MS spectrum acquisition, data-dependent acquisition (DDA) mode was employed, covering a range of m/z 70-1,000, and utilizing stepped normalized collision energies of 10, 20 and 40. The resolutions for the full mass scan and DDA were 70,000 and 17,500, respectively.

The R package XCMS (version 3.8.2; Posit Software) was used for peak detection, retention-time alignment, peak matching and correction. The R package statTarget (version 1.32.0; Posit Software) was used to filter for noisy ions that: i) Were not detected in >80% of all samples in any group; and ii) had an RSD of >30% in quality control (QC) samples. The k-nearest neighbors method was performed for missing values imputation, and then the QC-based random forest signal correction was used to correct the influence of the signal shift during LC-MS analysis. The R package, ropls (version 1.14.1; Posit Software), which included principal component analysis and partial least-squares discriminant analysis (PLSDA), was used for multivariate analysis. Metabolic features with a variable importance in the

Table III. The sequences of SLC7A5 shRNA and negative controls.

A, Human	
shRNA	Sequence (5'-3')
Negative control	CCTAAGGTTAAGTCGCCCTCG
SLC7A5 shRNA1	GGAAGGGTGATGTGTCCAA
SLC7A5 shRNA2	CCAATCTAGATCCCAACTT
B, Mouse	
Primer	Sequence (5'-3')
Negative control	TTCTCCGAACGTGTCACGT
SLC7A5 shRNA	CCTATTTCACTACCCTCTCTA

SLC7A5, solute carrier family 7 member 5; shRNA, short hairpin RNA.

projection score (VIP) >1, Benjamini-Hochberg adjusted P-value (false discovery rate) <0.05 and |log2 fold change|>2 were defined as differential features. Metabolite annotation was performed through matching the spectra (MS/MS) from the metabolite mass spectral (METLIN; http://metlin.scripps.edu), the Human Metabolome Database (HMDB; http://www.hmdb.ca/) and an in-house spectral database. The annotated metabolites were further enriched in metabolic pathways using MetaboAnalyst (https://www.metaboanalyst.ca) software.

Plasma metabolic profiling. A total of 100 μl of plasma was pipetted into an Eppendorf tube, an equal volume of 5% (v/v) perchloric acid solution was added and the solution was mixed thoroughly. The mixture stood at room temperature for 10 min to fully precipitate the proteins in the plasma. After which, the mixture was centrifuged at 10,000 x g for 10 min at 4˚C. Finally, 10 μl of the supernatant was aspirated for injection analysis. A DIONEX UltiMate 3000 (Thermo Fisher Scientific, Inc.) with a Thermo Hypersil GOLD column (100x2.1 mm, 1.9 μm) was used for chromatographic separation. The flow rate was set at 0.2 ml/min, and the column oven temperature was set at 30˚C. Mobile phase A was 15 mM sodium acetate buffer at pH 4.0, and mobile phase B was acetonitrile. A linear gradient was applied, in which percentage of B began in 0% and increased to 6% at 4 min, to 80% at 6 min and kept for 9 min, then returned to 0% at 10 min and held until 13 min. Samples were kept at 4˚C. The data were analyzed by Xcalibur (version 2.1.0; Thermo Fisher Scientific, Inc.).

Clonogenic assay. SKOV3 cells (500-1,000) were seeded in 6 cm dishes in culture medium containing 500 μM BCH or 100 μM JPH203 for clonogenic survival analysis. After 48 h, the cells were washed twice with complete culture medium to remove BCH and JPH203. Cells were then cultured in drug-free medium for 10-14 days, stained with 0.1% crystal violet for 15 min at room temperature and counted manually. Colonies consisting of >50 cells were considered viable and scored using a light microscope.

Cell cycle analysis. Cell cycle analysis was performed the cell cycle kit (cat. no CCS012; Multi Sciences (LIANKE) Biotech, Co., Ltd.). Harvested SKOV3 cells were washed with PBS, 1 ml of DNA holding solution and 10 μl of permeabilization solution was added and the sample was vortexed for 5 sec. The samples was incubated at room temperature in the dark for 30 min. The samples were analyzed by flow cytometry (Beckman CytoFLEX; Beckman Coulter, Inc.) and the data were analyzed using Cytomics™ FC500 software (Beckman Coulter, Inc.).

Immunohistochemistry (IHC) and immunofluorescence. The tissue were fixed with 4% formaldehyde for 24 h at room temperature and immunohistochemical staining was performed on 4-μm-thick formalin-fixed paraffin-embedded (FFPE) tumor samples. FFPE sections were dewaxed with xylene for 5 min and placed in 100, 95 and 75% ethanol at room temperature for hydrate for 5 min each time. Antigen retrieval was performed by heating the sections to 95˚C in citrate buffer (pH 6.0; cat. no. C1010; Beijing Solarbio Science & Technology Co., Ltd.) for 40 min. The sections were treated with 0.1% Triton 100 at room temperature for 10 min to break the membrane. The sections were washed twice with PBS for 5 min at room temperature. The sections were blocked with 5% goat serum (cat. no. SL038; Beijing Solarbio Science & Technology Co., Ltd.) for 30 min at room temperature. Tissues were incubated with primary antibodies for 1 h at room temperature, followed by incubation with Dako EnVision + System HRP-labeled polymer for 5 min at room temperature (Dako; Agilent Technologies, Inc.). Tissue samples were counterstained with hematoxylin at room temperature for 2 min, and then dehydrated with different concentrations of alcohol (75, 95 and 100%) for 5 min each time. Finally, the sections were, placed onto coverslips and imaged under an upright microscope. The antibodies used were: Anti-aryl hydrocarbon receptor (AHR; 1:500; cat. no. 67785-1-Ig; Wuhan Sanying Biotechnology), anti-SLC7A5 (1:200; cat. no. 28670-1-AP; Wuhan Sanying Biotechnology), anti-indoleamine 2,3-dioxygenase 1 (IDO1; 1:100; cat. no. 13268-1-AP; Wuhan Sanying Biotechnology) and arylformamidase (AFMID; 1:100; cat. no. 19533-1-AP; Wuhan Sanying Biotechnology). The tissue samples were manually categorized as: Negative, -; weak, +; medium, ++; and strong, +++, based on the degree of positive immunostaining staining.

Immunofluorescence staining was performed using 8-chamber slides. SKOV3cells were fixed with 4% paraformaldehyde for 15 min at room temperature, then washed three times with PBS for 5 min each time, permeabilized with 0.5% Triton-100 (Beijing Solarbio Science & Technology Co., Ltd.) and blocked with 5% BSA (Beijing Solarbio Science & Technology Co., Ltd.) for 1 h at room temperature. Cells were incubated with primary antibodies overnight at 4˚C, followed by incubation with fluorescent secondary antibodies at room temperature for 1 h at room temperature. Nuclear counterstaining was performed using DAPI (Beijing Solarbio Science & Technology Co., Ltd.) at room temperature for 10 min.

The primary antibodies used were: Anti-AHR (1:500; cat. no. 67785-1-Ig; Proteintech Group, Inc.) and anti-programmed death-ligand 1 (PD-L1; 1:300; cat. no. 66248-1-Ig; Proteintech Group, Inc.). The fluorescent secondary antibodies used were: iFluor™ 488 conjugated goat anti-mouse IgG goat polyclonal antibodies (1:1,000; cat no. HA1125; HUABIO) and iFluor™ 594 conjugated goat anti-mouse IgG Goat polyclonal antibodies (1:1,000; cat. no. HA1126; HUABIO).

Measurement of ^{13}C-Trp and ^{13}C-Kyn levels. SKOV3 parental cells and SLC7A5-shRNA knockdown SKOV3 cells were cultured in Trp-depleted MyCoy's 5A medium for 48 h. The cells were washed twice with the same medium before the addition of 1 μM ^{13}C-Trp and cells were harvested with a cell scraper following 5 min of incubation. Metabolites were extracted in 80% cold methanol and the extract was treated in vacuum freeze dryer for 6 h (-80˚C, 5 bar) to obtain the dry pellets. The dried pellets were used for cell-based LC-MS analysis as previously described (27).

Chromatin immunoprecipitation-quantitative PCR (ChIP-qPCR). ChIP-qPCR was performed using a ChIP Kit (cat. no. 56383S; CST Biological Reagents Co., Ltd.) according to the manufacturer's instructions. Briefly, SKOV3 cells (1x10^7 cells) were cross-linked with 1% formaldehyde for 10 min at room temperature. Fixed cells were lysed by 1X ChIP Sonication Cell lysis Buffer on ice for 10 min. The cells were centrifuged at 5,000 x g for 5 min at 4˚C. The supernatant was removed and cells were resuspended in ice-cold ChIP Sonication Nuclear lysis Buffer and incubated on ice for 10 min. The DNA of the sample was broken by a non-contact ultrasonic crusher (Covaris M220; Covaris, LLC) under the following ultrasonic conditions: PIP (75), duty factor (5%), CPB (200), treatment time (4 min), setpoint temperature (7˚C). Then the lysates were incubated with anti-AHR antibodies (1:50; cat. no. 83200s; CST Biological Reagents Co., Ltd.) at 4˚C overnight. After antibody incubation, ChIP-Grade Protein G magnetic beads were added and the sample was incubated for 2 h at 4˚C. After which, the magnetic beads were washed with cold PBS three times, for 5 min each. Proteinase K was added and incubated for 2 h at 65˚C to obtain the crude extract of DNA. After which, five times the volume of DNA Binding buffer was added and mixed gently, and the DNA sample was transferred to the DNA spin column at 4˚C for 17,000 x g centrifugation for 1 min. The DNA column was washed with Wash Buffer, and the liquid was discarded after 17,000 x g centrifugation at 4˚C for 1 min. Finally, DNA Elution Buffer was added to obtain purified DNA. The purified DNA were amplified by qPCR. The primers targeting the PD-L1 promoter were designed using Primer Premier (version 5; Premier Biosoft International) software (Table IV; Appendix S1). The master reaction mix was as follows: 6 μl nuclease-free H_2O, 2 μl primers (5 μM), 10 μl SYBR Green Master Mix (2X) and 2 μl DNA. The thermocycling conditions were as follows: Initial denaturation at 95˚C for 3 min, denaturing at 95˚C for 15 sec, and annealing and extension at 60˚C for 60 sec, denaturing, annealing and extension were repeated for a total of 40 cycles. The $2^{-\Delta\Delta Cq}$ formula (28) was used to calculate the relative expression levels of the target gene.

Table IV. The sequences of primers used for quantitative-PCR analysis of gene expression.

Primer	Sequence (5'-3')
PD-L1-P1	F: GAATAGGAAGTGGTGGTA
	R: TGGACGAAATAGATGGAG
PD-L1-P2	F: AAAATGAATGGCTGAAGG
	R: AAAGTTGCTGATGGGAAT
PD-L1-P3	F: GCTCTGAAGCCAGTTGTT
	R: CTGCAATGCCCTCTGATA
PD-L1-P4	F: CAACTTCGGGAACTTTGG
	R: CTTGATTTGGCAGGAGCA
PD-L1-P5	F: AAGGAAAGGCAAACAACG
	R: AAGTGATCCGCCAAAGTG
PD-L1-P6	F: GCCCATTCACTAACCCAA
	R: CCTGATATTCTGCCACCC
PD-L1-P7	F: TCAGATGTTGGCTTGTTG
	R: TTTCACCGGGAAGAGTTT

PD-LI, programmed death ligand 1.

Immunoblotting. Whole cell lysates were prepared using RIPA Lysis Buffer (Beyotime Institute of Biotechnology) containing 1 mM phenylmethylsulfonylfluoride. Cytoplasmic and nuclear fractions were isolated using an NE-PER™ kit (Thermo Fisher Scientific, Inc.). A BCA kit (Beyotime Institute of Biotechnology) was used to determine the protein concentration. Next, 30 μg of protein lysate from each sample was loaded into each lane of a 10% SDS-PAGE gel, electrophoresed and transferred to a PVDF membrane. The membranes were blocked with 5% non-fat milk for 1 h at room temperature and washed three times at room temperature with TBST for 10 min each time. After which, the samples incubated with the primary antibodies overnight at 4˚C. The next day, the membranes were washed three times at room temperature with TBST for 10 min and incubated with the respective secondary antibodies at room temperature for 1 h and detected using an ECL reagent (cat. no. FD8000; Fdbio Science) with the ChemiDOC™ XRS + (Bio-Rad Laboratories, Inc.). The primary antibodies used were: Anti-AHR (1:1,000 dilution; cat. no. 67785-1-Ig; Proteintech Group, Inc.), anti-SLC7A5 (1:1,000; cat. no. 28670-1-AP; Proteintech Group, Inc.), anti-PD-L1 (1:1,000; cat. no. 66248-1-Ig; Proteintech Group, Inc.), anti-histone H3 (1:10,000, cat. no. 68345-1-Ig; Proteintech Group, Inc.), anti-tubulin (1:5,000; cat. no. 11224-1-AP; Proteintech Group, Inc.) and anti-GAPDH (1:5,000; cat. no. 10494-1-AP; Proteintech Group, Inc.). Tubulin was used as the cytoplasmic reference, histone H3 as the nuclear reference and GAPDH as the whole cell reference. The secondary antibodies were as follows: Anti-rabbit IgG (1:3,000; cat. no. 7074; CST Biological Reagents Co., Ltd.) and anti-mouse IgG (1:3,000; cat. no. 7076; CST Biological Reagents Co., Ltd.)

T cell co-culture with ovarian cancer cells. CD3$^+$ T cells were magnetically isolated from peripheral blood mononuclear cells (PBMCs) through Ficoll-Paque density gradient centrifugation

of peripheral blood derived from healthy adult donors. Briefly, 10 ml of peripheral blood was diluted with PBS (containing 0.5% BSA) in a 1:1 ratio. Next, 5 ml of Ficoll-Paque PLUS was added into a new centrifuge tube and diluted blood cells were added to the upper layer of the tube. The sample was centrifuged at 800 x g for 20 min at room temperature to separate the PBMCs. $CD3^+$ MicroBeads human (Miltenyi Biotec GmbH), LS columns (Miltenyi Biotec GmbH) and a MACS®MultiStand separator (Miltenyi Biotec GmbH) were used to magnetically separate $CD3^+$ cells from PBMCs according to the manufacturer's protocol. Once $CD3^+$ T cells were isolated from PBMCs, they were activated using 0.5 μg/ml anti-CD3 (cat. no. 555336; Becton, Dickinson and Company), 5 μg/ml anti-CD28 (cat. no. 555725, Becton, Dickinson and Company) and 100 U/ml IL-2 (cat. no. 200-02-10UG; PeproTech, Inc.) antibodies for 48 h (37˚C, 5% CO_2). Preactivated T cells were then co-cultured with SKOV3 cells at a ratio of 5:1 for 48 h. Hoechst 33324 (Sigma-Aldrich; Merck KGaA) staining for 10 min at room temperature was performed to observe T cell localization. Changes in cell morphology were detected using fluorescence microscopic imaging.

CCK-8 assay. Cell survival rates were measured using a CCK-8 assay (Beyotime Institute of Biotechnology). Preactivated T cells and SKOV3 cells were co-cultured in 96-well plates at a ratio of 5:1 for 48 h, after which the supernatant was discarded and 100 μl of culture medium containing 10% CCK-8 (Beyotime Institute of Biotechnology) was added and incubated for 2 h. The absorbance was measured at 450 nm using a microplate reader (Varioskan Flash; Thermo Fisher Scientific, Inc.).

In vivo tumorigenicity. A total of 16 female BALB/c nude mice (age, 4 weeks; body weight, 16-18 g) were purchased from the Shanghai Laboratory Animal Center. Animals were maintained in pathogen-free facilities at the Zhejiang Cancer Hospital, under a controlled environment (temperature, 23±1˚C; humidity, 50±5%; 12/12 h light/dark cycle), provided with standard laboratory chow and free access to purified water. All experiments were conducted in accordance with the National Institutes of Health Guide for the Care and Use of Laboratory Animals and approved by the Zhejiang Cancer Hospital Laboratory Animal Ethics Committee (approval no. 2021-05-003; Hangzhou, China). Parental SKOV3 cells or SKOV3 cells transfected with shSLC7A5 were injected into the left flank of mice, at a concentration of $5x10^6$ cells in 100 μl in PBS/Matrigel mixed in a 1:1 ratio. The tumor diameters were measured every 3 days for 3 weeks. Tumor length was not permitted to exceed 10 μm during this time period. The mice were then anesthetized using an intraperitoneal (i.p.) injection of sodium pentobarbital (50 mg/kg), sacrificed by cervical dislocation and the tumors were isolated. Euthanasia was confirmed by the lack of movement including respiration and heartbeat.

To investigate the efficacy of immunotherapy, a total of 20 female C57BL/6 mice (age, 4 weeks; body weight, 16-18 g) were purchased from the Shanghai Laboratory Animal Center. Parental ID8 cells or ID8 cells stably expressing shSLC7A5 were injected into the left flank of mice, at a concentration of $2x10^6$ cells in 100 μl in PBS/Matrigel mixed in a 1:1 ratio. PD-1 monoclonal antibodies were diluted with normal saline (1:200; cat. no. BE0146; BioXCell) and 10 mg/kg injected (i.p.) twice per week. The tumor diameter was measured every 5 days and the tumor volumes were calculated using the formula: (Length x $width^2$)/2. Tumor length was not permitted to exceed 10 mm. After 5 weeks, the mice were anesthetized using sodium pentobarbital (50 mg/kg, i.p.), sacrificed by cervical dislocation and the tumors were isolated.

Statistical analysis. Statistical analyses were performed using SPSS software 18.0 (IBM Corp.) and GraphPad software 9.0 (Dotmatics) software. Comparison analysis was performed using with an unpaired Student's t-test between two groups or a one-way ANOVA with Dunnett's post hoc test on >2 groups. Kaplan-Meier curves were used to identify associations between metabolites and PFS using median split and log-rank tests. Cox proportional hazards regression analysis was performed for analysis of metabolites. All statistical tests were two-sided and $P<0.05$ was considered to indicate a statistically significant difference.

Results

Increased expression levels of Trp importers and pathway enzymes in ovarian cancer. To investigate the regulatory roles of the Trp metabolism pathway in the context of increased Kyn expression levels demonstrated in patients with ovarian cancer (29), changes in the protein and enzyme expression levels that are involved in Trp uptake and/or Trp-catabolic processes were examined. Analysis using the Cancer Genome Atlas (TCGA; http://gepia.cancer-pku.cn/) database demonstrated increased expression levels of SLC7A5 (Fig. 1A), IDO1 (Fig. 1B) and AFMID (Fig. 1C) in tissue samples from patients with ovarian cancer compared with healthy tissue samples. High mRNA expression levels of SLC7A5 (Fig. 1D), IDO1 (Fig. 1E) and AFMID (Fig. 1F) were associated with tumor stage, although only the expression levels of SLC7A5 were associated with tumor stage variation. IHC staining demonstrated increased protein expression levels of SLC7A5, IDO1 and AFMID in tissue samples from patients with ovarian cancer compared with benign ovarian cysts (Fig. 1G). The expression of SLC7A5 was positive in most tumor tissues, but negative in only a few benign cysts (Fig. 1H). Therefore, SLC7A5 was chosen for further investigation in the present study. SKOV3 and ES-2 cells treated with the SLC7A5 inhibitors BCH (500 μM) and JPH203 (100 μM) demonstrated significantly decreased Trp and Kyn expression levels compared with control cells, through LC-MS analyses (Fig. 1I and J). Tracking experiments using ^{13}C-Trp and ^{13}C-Kyn in SKOV3 control and SLC7A5-shRNA cells showed that knockdown of SLC7A5 expression levels led to a significant decrease in cellular ^{13}C-Trp and ^{13}C-Kyn expression levels compared with control cells (Fig. 1K and L).

SLC7A5 exhibited anti-ovarian cancer activity in vitro and in vivo. The antitumor effects of SLC7A5 in ovarian cancer tissues were tested *in vitro* and *in vivo*. SKOV3 cells were treated with either BCH (500 μM) or JPH203 (100 μM), which both significantly inhibited clonogenesis in SKOV3 cells (Fig. 2A). SLC7A5 knockdown in SKOV3 cells similarly demonstrated

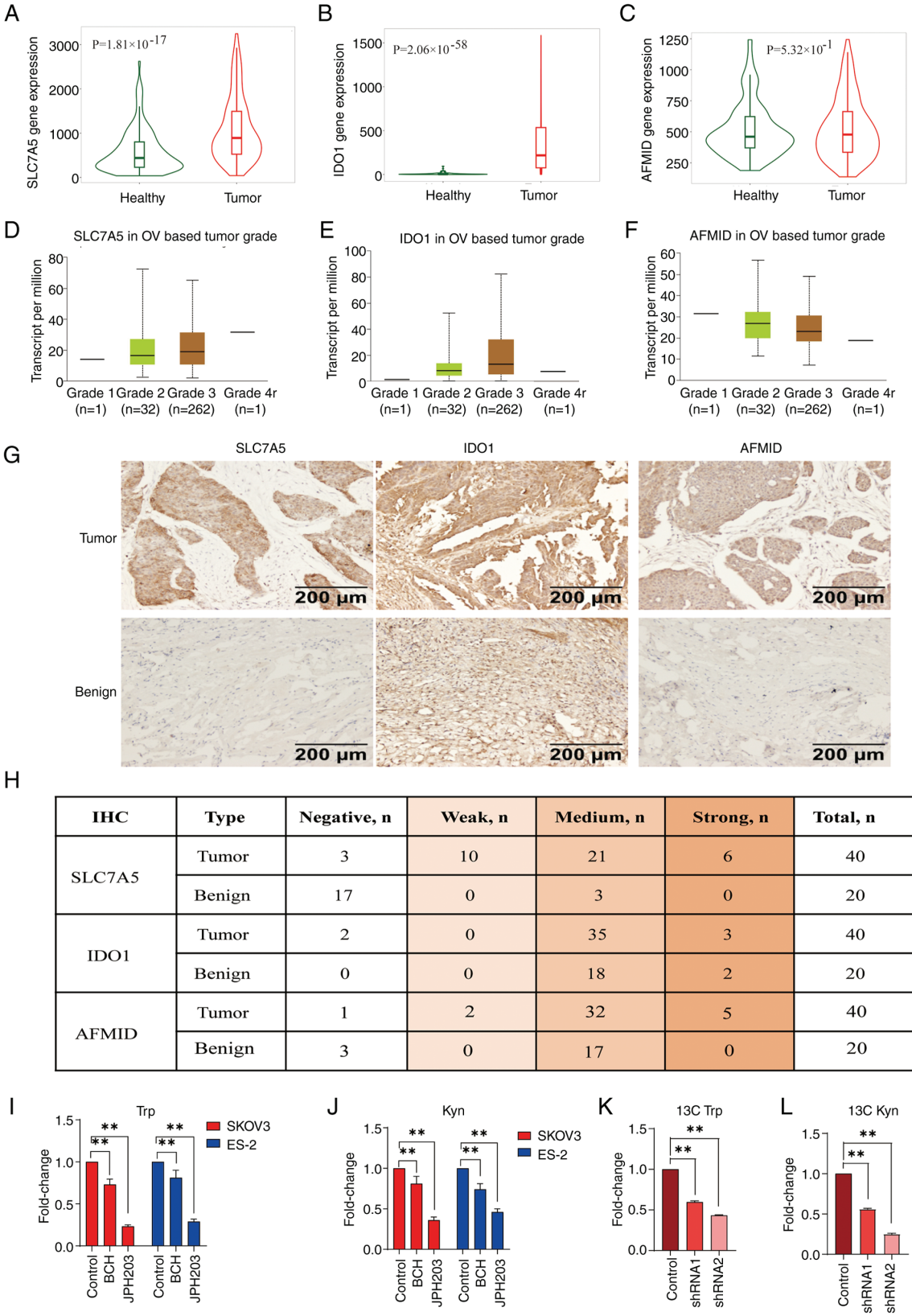

H

IHC	Type	Negative, n	Weak, n	Medium, n	Strong, n	Total, n
SLC7A5	Tumor	3	10	21	6	40
	Benign	17	0	3	0	20
IDO1	Tumor	2	0	35	3	40
	Benign	0	0	18	2	20
AFMID	Tumor	1	2	32	5	40
	Benign	3	0	17	0	20

Figure 1. Increased expression levels of Trp importers and enzymes in the Trp pathway in ovarian cancer. Violin plots of mRNA expression levels of (A) SLC7A5, (B) IDO1 and (C) AFMID in tissue samples from patients with ovarian cancer compared with healthy tissues from The Cancer Genome Atlas ovarian cancer database. The mRNA expression levels of (D) SLC7A5, (E) IDO1 and (F) AFMID were expressed in different tumor stages. (G) Representative images of IHC staining of SLC7A5, IDO1 and AFMID in ovarian cancer tissue samples (n=40) and benign cysts (n=20). (H) Quantification of IHC staining of SLC7A5, IDO1 and AFMID in tissue samples from patients with ovarian cancer (n=40) and benign cysts (n=20). LC-MS quantification of cellular (I) Trp and (J) Kyn expression levels in SKOV3 and ES-2 cells treated with BCH (500 μM) or JPH203 (100 μM) for 48 h. LC-MS/MS quantification of cellular (K) ^{13}C-Trp and (L) ^{13}C-Kyn in SKOV3 cells transfected with either control shRNA or shRNA targeting SLC7A5. **P<0.01; n=3. Data are presented as mean ± SD. shRNA, short hairpin RNA; IHC, immunohistochemistry; LC-MS/MS, liquid chromatography-tandem mass spectrometry; LC-MS, liquid chromatography-mass spectrometry; OV, ovarian; Trp, tryptophan; Kyn, kynurenine; SLC7A5, solute carrier family 7 member 5; IDO1, indoleamine 2,3-dioxygenase 1; AFMID, arylformamidase.

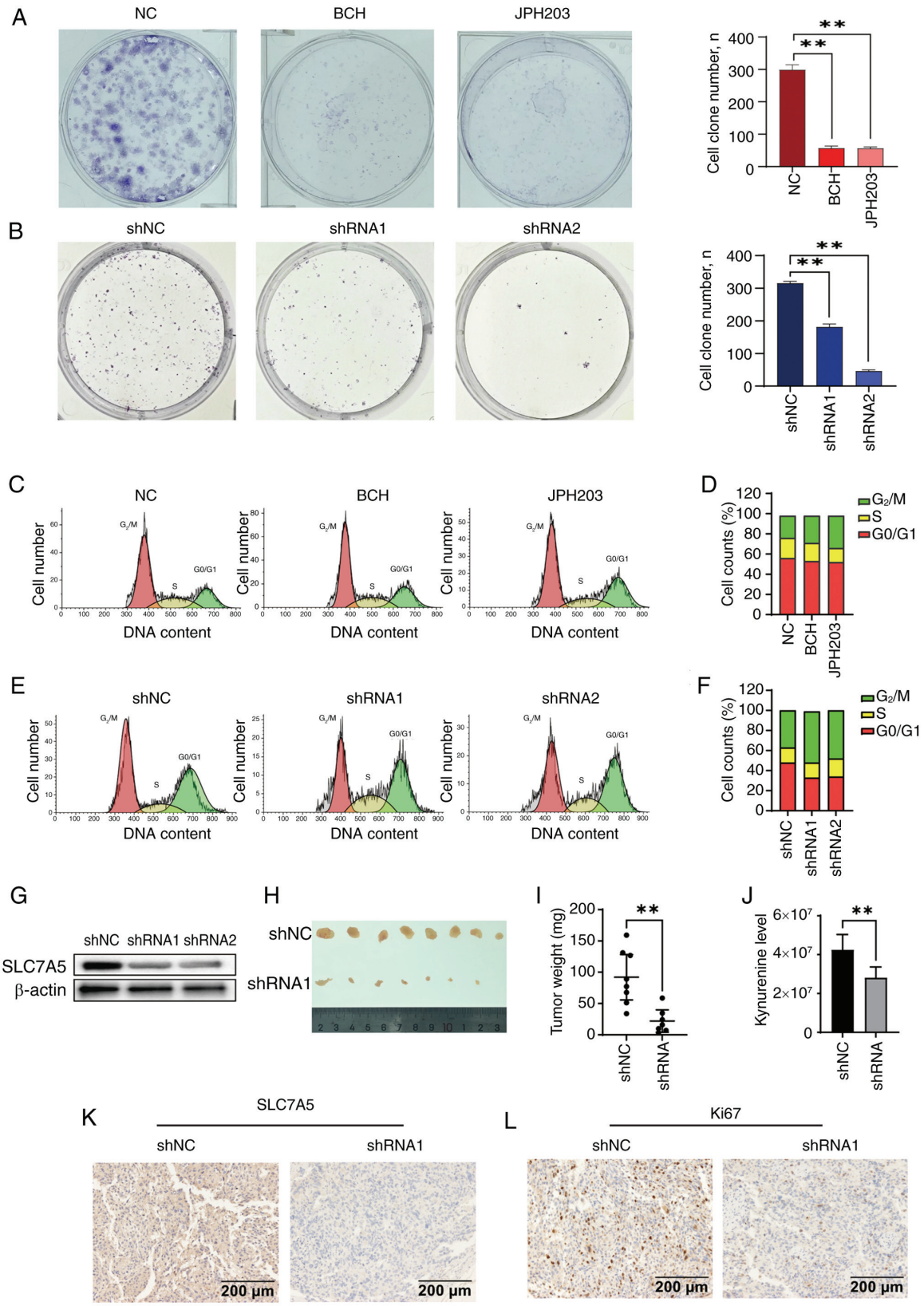

Figure 2. SLC7A5 showed anti-ovarian cancer activity *in vitro* and *in vivo*. The representative images and quantitative analyses of clonogenic survival assay results of control and shSLC7A5 SKOV3 cells treated with either (A) BCH (500 μM) or (B) JPH203 (100 μM). (C) The representative distribution of SKOV3 cells in the cell cycle phases, treated with either BCH (500 μM) or JPH203 (100 μM) for 48 h as analyzed by flow cytometry. (D) The percentage of SKOV3 cells in the cell cycle phases, treated with either BCH (500 μM) or JPH203 (100 μM) for 48 h. (E) The representative distributions of SKOV3 shSLC7A5 cells in the cell cycle phases analyzed by flow cytometry. (F) The percentages of SKOV3 shSLC7A5 cells at each phase of the cell cycle. (G) The expression of SLC7A5 from SKOV3 cells transfected with control shRNA or shSLC7A5 by western blotting. (H) The tumor size and (I) weight of SKOV3 transfected with control shRNA (scramble) or shSLC7A5 inoculated in BALB/c nude mice. (J) LC-MS/MS quantification of Kyn in serum of BALB/c nude mice bearing SKOV3 transfected with control shRNA or sh-SLC7A5. Immunohistochemical staining of (K) SLC7A5 and (L) Ki67 in xenograft tumors from BALB/c nude mice bearing SKOV3 transfected with control shRNA or sh-SLC7A5. **P<0.01; n=8. Data are presented as mean ± SD. shRNA, short hairpin RNA; NC, negative control; LC-MS/MS, liquid chromatography-tandem mass spectrometry; Kyn, kynurenine; SLC7A5, solute carrier family 7 member 5.

inhibition of clonogenesis (Fig. 2B). Flow cytometry showed that treatment with the SLC7A5 inhibitors, BCH (500 μM) or JPH203 (100 μM), were associated with G_2/M phase arrest in SKOV3 cells (Fig. 2C and D) and in SKOV3 shSLC7A5 cells (Fig. 2E and F). SLC7A5 expression levels were notably decreased using the SLC7A5 shRNA in SKOV3 cells (Fig. 2G).

The *in vivo* tumor model demonstrated a significant decrease in tumorigenesis in the SLC7A5-shRNA engineered SKOV3 xenograft tumors (shSLC7A5) group compared with control mice with the parental SKOV3 xenograft shNC) group (Fig. 2H and I). Kyn expression levels were decreased in the serum of the shSLC7A5 group compared with that in the shNC group (Fig. 2J). IHC results demonstrated decreased SLC7A5 expression levels in the shSLC7A5 group compared with the shNC group (Fig. 2K). Silencing of SLC7A5 expression levels in SKOV3 cells was associated with decreased Ki67 expression levels in the shSLC7A5 group compared with the shNC group (Fig. 2L).

Kyn increased nuclear AHR and PD-L1 expression levels in ovarian cancer cells. Analysis using the TCGA database showed a significant correlation between SLC7A5 with AHR and PD-L1 expression levels in ovarian cancer (Fig. 3A). IHC analysis of AHR expression levels in ovarian cancer and benign ovarian cyst tissue samples showed increased AHR staining in the nuclei of ovarian cancer cells when compared with ovarian benign cyst tissue samples (Fig. 3B).

The effects of cellular Kyn levels on the localization and expression of AHR and PD-L1 in PDC and SKOV3 ovarian cancer cells were examined through the manipulation of Kyn concentrations in the cell culture medium and were determined by immunofluorescence and immunoblotting, respectively. The addition of 20 μM Kyn to the culture medium 30 min prior to cell collection significantly decreased the cytoplasmic AHR protein expression levels and increased nuclear AHR protein expression levels in SKOV3 and PDC cells, which indicated that Kyn could promote AHR translocation to the nucleus (Fig. S1A and B). Compared with control cells, the addition of 20 μM Kyn upregulated the protein expression levels of PD-L1 and AHR in SKOV3 and PDC cells (Fig. S1C and D). Immunofluorescence staining showed increased nuclear staining of AHR after cells were treated with 20 μM Kyn compared with control cells (Fig. S1E).

The ability of Kyn to increase the nuclear translocation of AHR was significantly decreased when the cells were co-treated with JPH203 (Fig. 3C). Silencing of SLC7A5 in shSLC7A5 SKOV3 cells significantly decreased the nuclear AHR protein expression levels and the total protein expression levels of AHR and PD-L1 in SKOV3 cells compared with the shNC group, as demonstrated through immunoblotting (Fig. 3D and E). Immunofluorescent staining showed decreased nuclear translocation of AHR upon Kyn treatment in shSLC7A5 SKOV3 cells compared with the shNC SKOV3 cells (Fig. 3F). ChIP-qPCR demonstrated that 20 μM Kyn activated the binding of AHR to the PD-L1 promoter, which significantly upregulated PD-L1 expression levels compared with untreated SKOV3 cells (Fig. 3G and H). These results indicated that SLC7A5 may serve as an important regulator of the innate immune response in cancer cells.

Kyn inhibited the inhibitory interaction of T cells on SKOV3. To investigate if Kyn could affect the cytotoxic activity of T cells on ovarian cancer cells, SKOV3 cells were co-cultured with preactivated T cells in cell culture media with or without Kyn and the cell survival rate was assessed. These results showed that reactivated T cells aggregated at the edges of tumor cells. Furthermore, lysed SKOV3 cells and the reduced proliferation of SKOV3 cells in the co-culture system were observed. By contrast, T cell function in the co-culture system supplemented with Kyn was reduced compared with that in the control group (Fig. S2A). Kyn supplementation significantly decreased the cell survival rate of SKOV3 cells by ~27.8% compared with control cells without Kyn supplementation (Fig. S2B).

SLC7A5 increased the effects of PD-1 immunotherapy in ovarian cancer. The immune regulatory functions of SLC7A5 were examined *in vivo*. C57BL/6 mice were subcutaneously injected with either ID8 cells treated with control shRNA or shSLC7A5 and treated with PD-1 therapy. Tumors with shSLC7A5-treated ID8 cells showed significantly decreased tumorigenesis (Fig. 4A and B) and increased efficacy of anti-PD-1 antibody treatment (Fig. 4C). The results of IHC showed that compared with the shNC group, the expression of Ki67 and PDL1 in shRNA group decreased, while the expression of CD3 increased (Fig. 4D).

Disordered Trp metabolism and Trp as a novel prognostic marker and therapeutic target in ovarian cancer. To evaluate the association between Trp metabolism and ovarian cancer, a total of 117 tissue samples were obtained from patients, which included 77 tissue samples of advanced serous ovarian cancer and 40 of benign cysts. PLSDA score plots with ion features from LC-MS analysis demonstrated a notable separation between malignant and benign ovarian tissues (Fig. 5A). Differential ion features were defined as VIP >1, |log2Fold change|>0.585 and P<0.05. In the positive mode, 1,181 ion features were downregulated and 1,531 metabolites were upregulated, while 985 ion features were downregulated and 1,309 metabolites were upregulated in the negative mode (Fig. 5B). Through matching the MS1 and MS2 spectra with the reference metabolites from the HMDB and METLIN databases, 35 differential metabolites were annotated (Fig. 5C). Metabolomic Enrichment Analysis was performed using MetaboAnalyst and the top five enriched pathways were: Trp, methylhistidine, arginine and proline, glycine and serine and pyrimidine metabolic pathways (Fig. 5D). As the most enriched pathway, the Trp metabolic pathway had a total of six metabolites, which included Kyn, Trp, 5-hydroxyindoleaceyic acid, formylkynurenine, flavin adenine dinucleotide (FAD) and S-adenosylhomocysteine (Figs. 5E; S3A-E). The MS spectra of Kyn, Trp, 5-hydroxyindoleaceyic acid, formylkynurenine, FAD and S-adenosylhomocysteine were generated (Fig. S1K-P).

Among the five metabolite hits in the Trp pathway, the difference in multiplicity of formylkynurenine was the largest (Fold Change=9.24). The receiver operating characteristic (ROC) curve analysis showed the area under the curve (AUC) value of formylkynurenine to be 0.89 and the optimal cut-off value was 3.009 (Fig. 5F). The AUC values of Kyn, Trp, 5-hydroxyindoleaceyic acid, formylkynurenine, FAD and S-adenosylhomocysteine additionally were analyzed (Fig. S3F-J). Using reagent grade L-Trp and L-Kyn as standards,

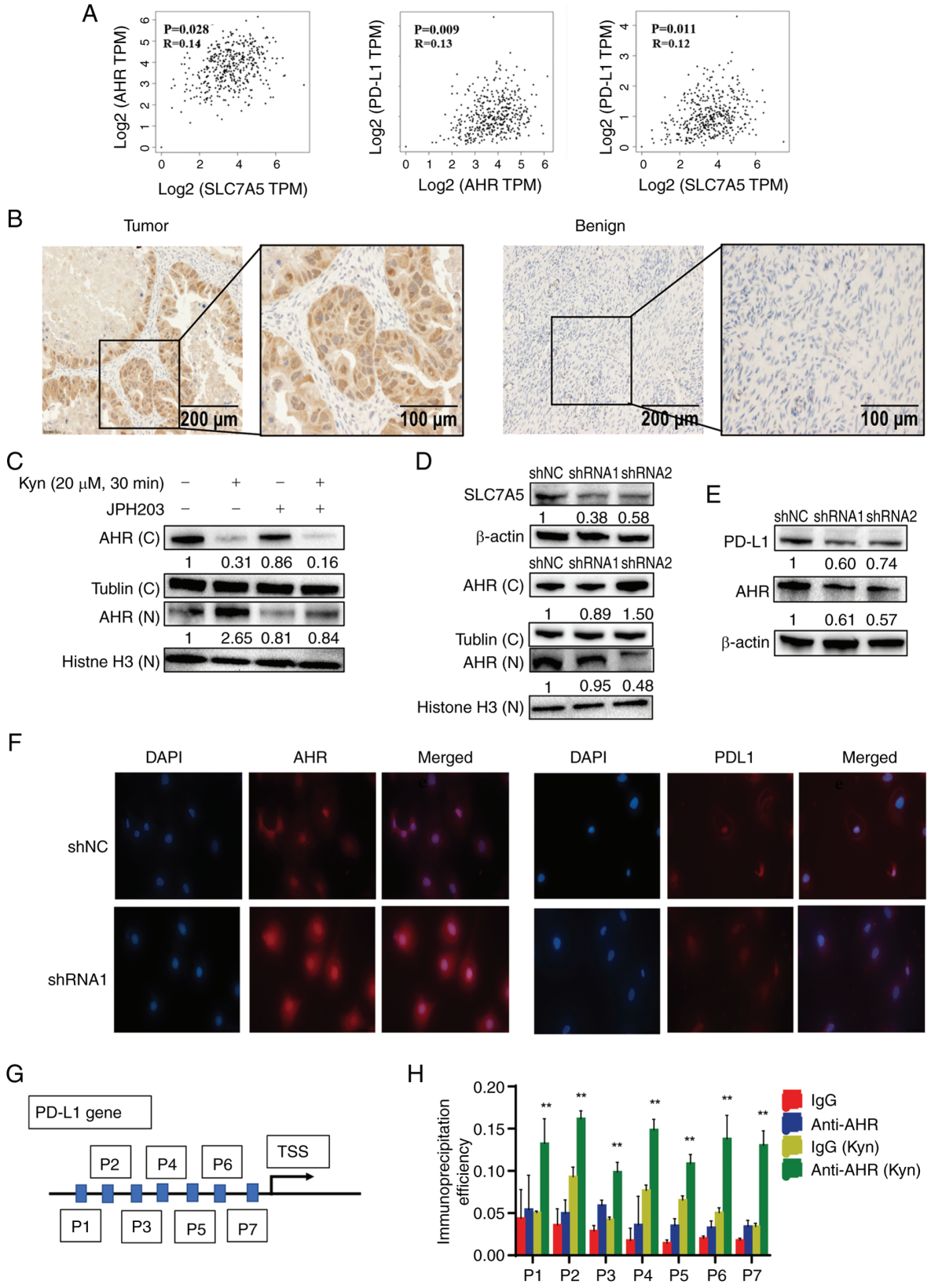

Figure 3. SLC7A5 affected Trp metabolism and PD-L1 expression levels. (A) Correlation between SLC7A5 with AHR and PD-L1 in human ovarian cancer, obtained from The Cancer Genome Atlas database. (B) Immunohistochemistry staining of AHR in ovarian cancer and benign ovarian cysts. (C) The expression of nuclear and cytoplasmic AHR from SKOV3 cells treated with 20 μM Kyn and SLC7A5 inhibitor JPH203 by western blotting. (D) The expression of nuclear and cytoplasmic AHR from SKOV3 cells transfected with sh-SLC7A5 or control by western blotting. (E) The expression of PD-L1 and AHR from SKOV3 cells transfected with control shRNA or shSLC7A5 by western blotting. (F) The immunofluorescence localization of AHR (red) and PD-L1 (red) in control or shSLC7A5 SKOV3 cells. Nuclei were counterstained with DAPI (blue). (G) The schematic diagram of predicted AHR binding sites in the PD-L1 promoter. (H) Chromatin-immunoprecipitation analysis of AHR binding to the PD-L1 promoter in SKOV3 cells treated with Kyn. Samples were normalized to the amount of input DNA, **P<0.01, n=3. Data are presented as mean ± SD. TPM, transcripts per million; TSS, transcription start site; shRNA, short hairpin RNA; C, cytoplasmic fraction; N, nuclear fraction; Trp, tryptophan; Kyn, kynurenine; SLC7A5, solute carrier family 7 member 5; AHR, aryl hydrocarbon receptor; PD-LI, programmed death ligand 1.

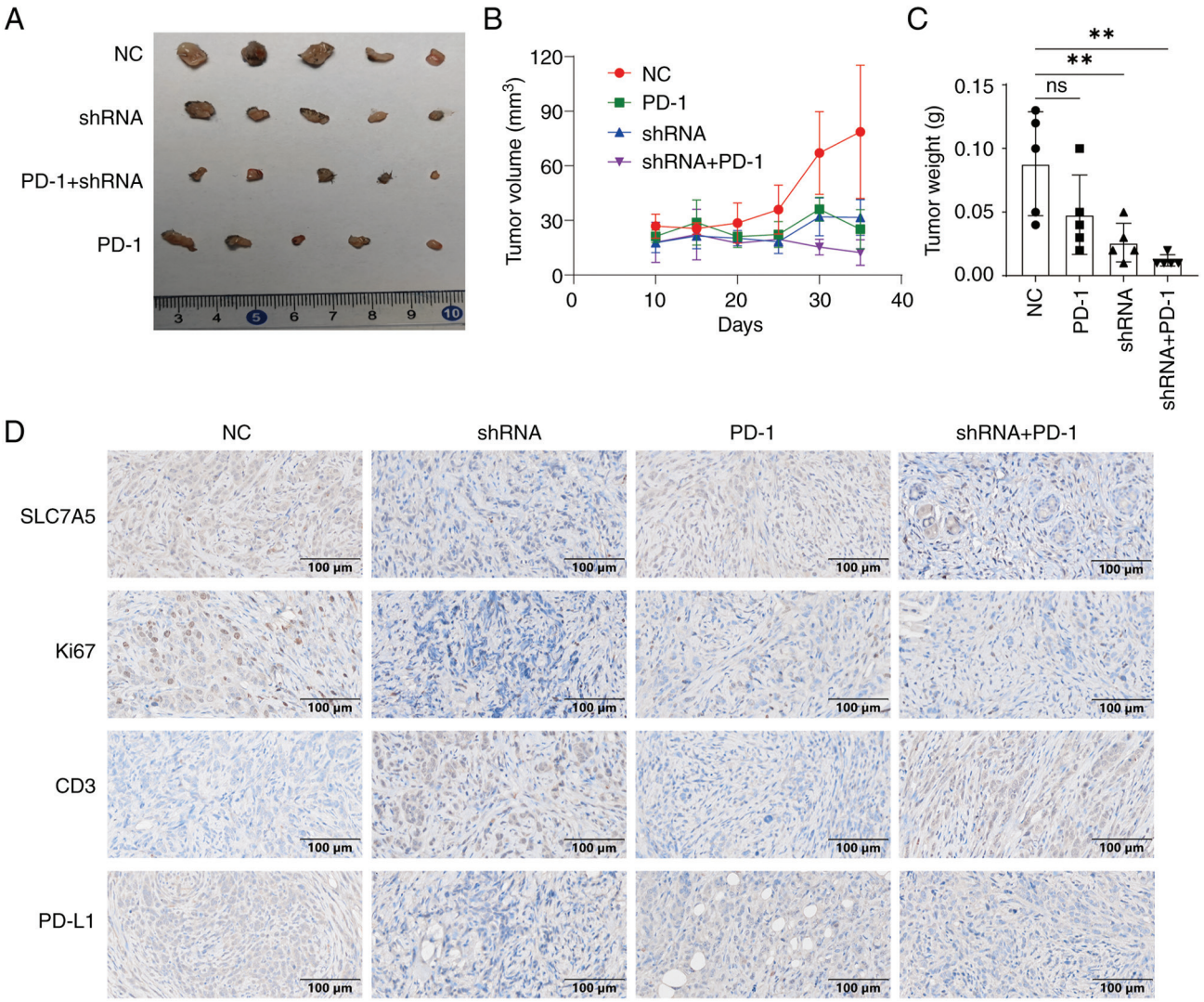

Figure 4. Knockdown of SLC7A5 increased PD-1 immunotherapy efficacy in ovarian cancer. (A) The expression of SLC7A5 from ID8 cells transfected with control shRNA or shSLC7A5 by western blotting. Representative images of tumor from four groups of C57BL/6 mice inoculated with either control shRNA ID8 cells, shSLC7A5 SKOV3, PD-1 monotherapy or shSLC7A5 ID8 cells combined with PD-1 therapy. Comparison of the (B) tumor volume and (C) weight of all groups. (D) The immunohistochemical staining of SLC7A5, Ki67, CD3 and PD-L1 protein in tumor from all four groups. **P<0.01, n=5. Data are presented as mean ± SD. shRNA, short hairpin RNA; NC, negative control; ns, not significant; SLC7A5, solute carrier family 7 member 5; PD-1, programmed death-1; PD-LI, programmed death ligand 1.

LC-MS analysis was performed to measure Trp and Kyn expression levels in the plasma specimens. Significantly decreased Trp and increased Kyn expression levels were detected in the plasma of patients with ovarian cancer compared with plasma samples from healthy donors (Fig. 5G and H). Follow-up information from 104 of the aforementioned patients were obtained. There were 51 cases with a Trp expression levels <600.79 and 53 cases with a Trp expression levels >600.79. Furthermore, there were 56 cases with a Kyn expression levels <62.97 and 48 cases with a Kyn expression levels >62.97. PFS analyses demonstrated that patients with lower Kyn expression levels detected in the plasma had longer PFS compared with those with high Kyn expression levels. However, no correlation between PFS and Trp expression levels was demonstrated (Fig. 5I and J).

Discussion

Tumor cells undergo metabolic reprogramming, a process where they alter their energy-producing pathways and nutrient utilization to sustain their rapid and uncontrolled growth (30). The present study indicated that ovarian cancer cells have an increased ability to take up Trp and process it through the Kyn pathway. It was demonstrated that the Trp transporter SLC7A5 served vital roles in Trp uptake and could inhibit the proliferation of ovarian cancer cells through regulation of the cell cycle. It was additionally demonstrated that the transcription factor AHR could be activated by Kyn to increase PD-L1 expression levels.

A rewired cellular metabolism is considered to be a notable hallmark of cancer. Abnormalities in Trp metabolism have been detected in certain types of cancers (including liver cancer, myeloma and breast cancer) and are recognized as important microenvironmental factors that can influence the immune responses of the tumor (31). Previous studies have demonstrated activation of the catabolic Kyn pathway in certain types of tumors and the potential for targeting Kyn catabolism for cancer therapy (32). The present study demonstrated that patients with ovarian cancer with low

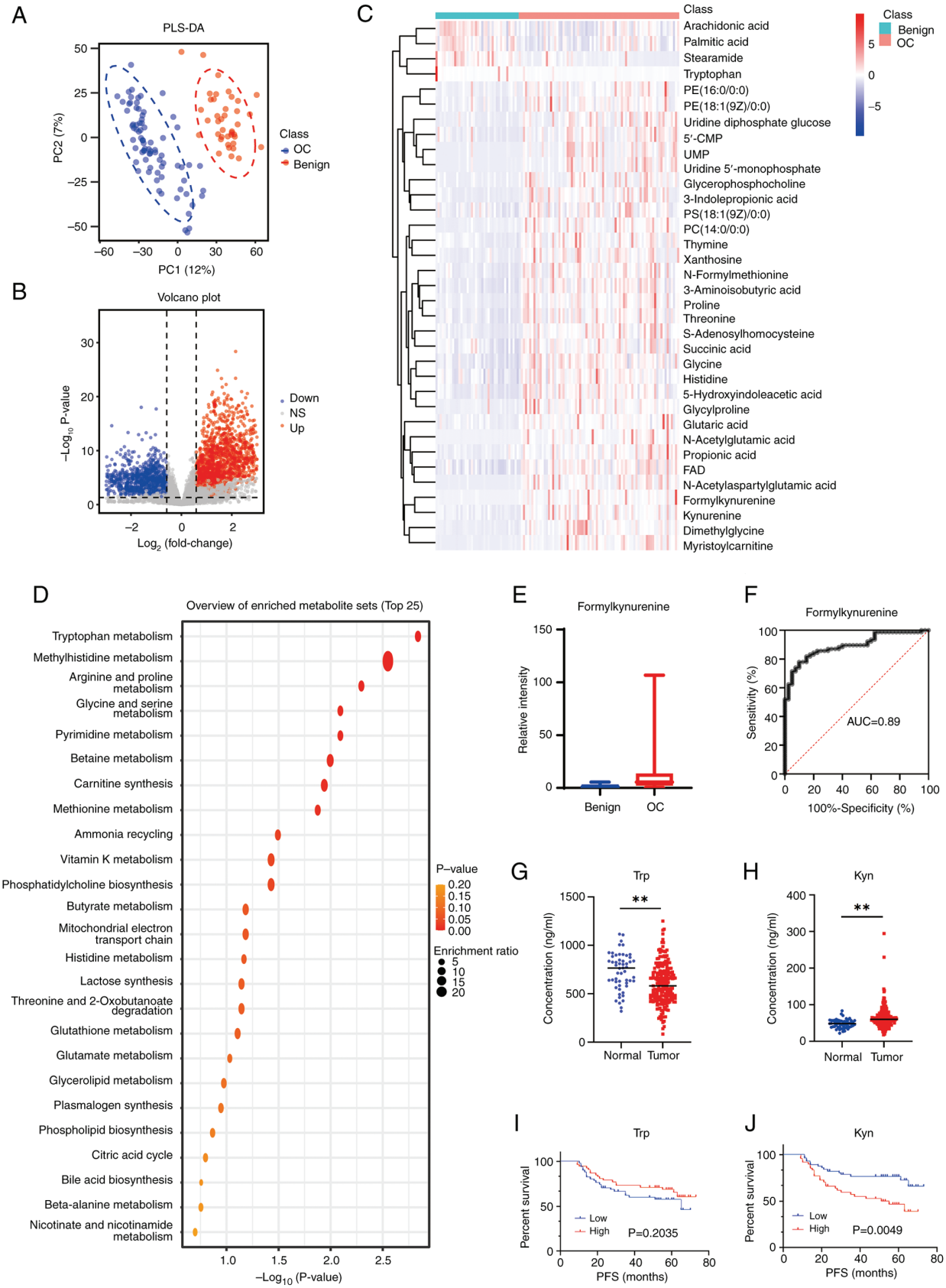

Figure 5. Metabolic differences in ovarian cancer and benign cysts. (A) Positive ion score plot derived from partial least squares discriminant analysis among OC and benign tissues. (B) Differential positive ion features were defined between OC and benign tissues, variable importance in the projection score >1, fold change >1.5, fold change <0.667 and P<0.05. (C) Heatmap analysis with 35 differential metabolites demonstrated a separation in metabolic pattern between OC and benign tissues. (D) Pathway analysis of 35 differential metabolites with the 35 most significant metabolism pathways. (E) The levels of formylkynurenine in ovarian cancer and benign tissues. (F) The receiver operating characteristic curve of the formylkynurenine for OC. The levels of (G) Trp and (H) Kyn in plasma of patients with OC (n=202) and healthy individuals (n=54). **P<0.01. Data are presented as mean ± SD. The PFS of patients with high and low (I) Trp and (J) Kyn level. PC1, principal component 1; PC2, principal component 2; PLS-DA, principal component analysis and partial least-squares-discriminant analysis; AUC, area under the curve; OC, ovarian cancer; NS, not significant; PFS, progression-free survival; Trp, tryptophan; Kyn, kynurenine.

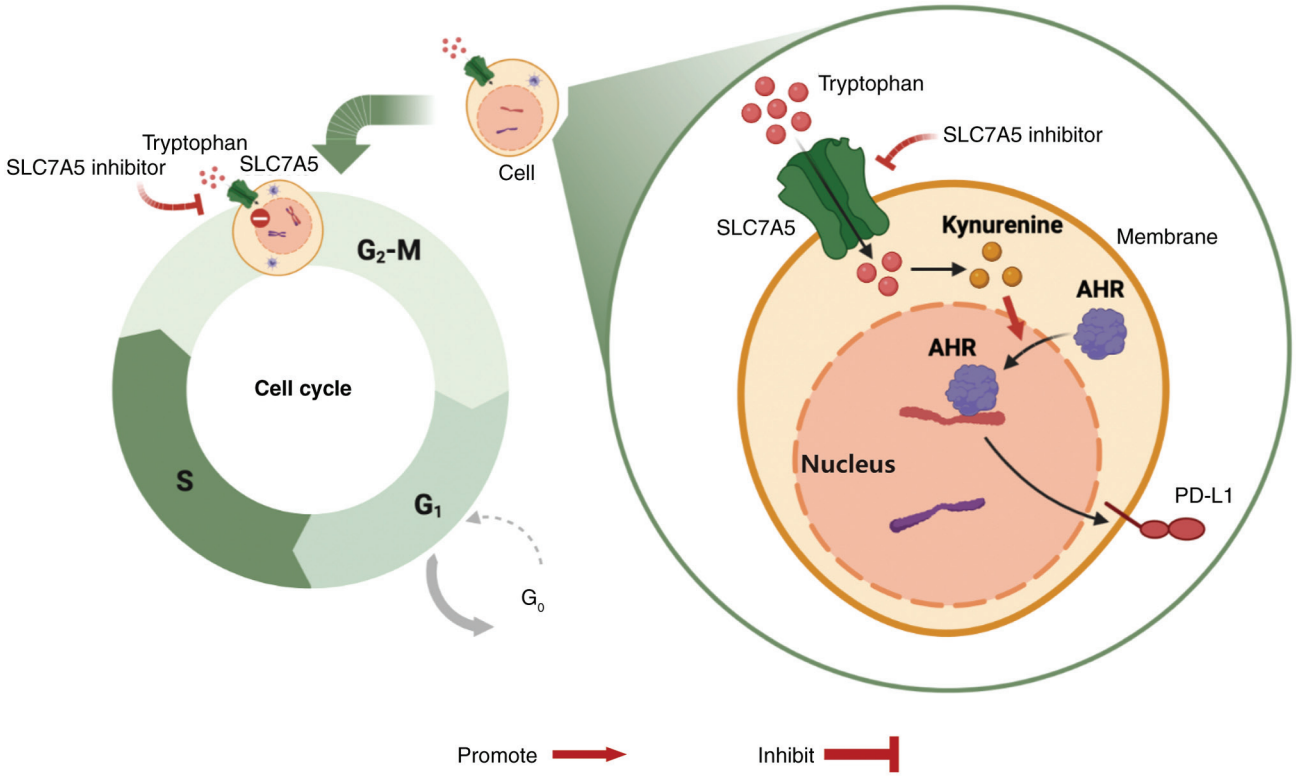

Figure 6. SLC7A5 arrested the cell cycle at the G_2/M phase of the cell cycle and increased PD-L1 expression levels by regulating the tryptophan-kynurenine-AHR axis in ovarian cancer. SLC7A5, solute carrier family 7 member 5; AHR, aryl hydrocarbon receptor; PD-LI, programmed death ligand 1.

plasma Kyn expression levels had a longer PFS compared with those with high Kyn expression levels. Therefore, the reduction of Kyn expression levels may potentially be an important strategy for the treatment of patients with ovarian cancer. Catabolism of the Kyn pathway involves several key enzymes, such as IDO1, IDO2, Trp 2,3-dioxygenase (TDO) and AFMID (33). However, a number of IDO1 inhibitors have failed in previous preclinical and clinical trials (34,35). A potential explanation is that when IDO1 is inhibited in tumor cells, TDO activity compensates for Trp metabolism and promotes Kyn production (36). The present study showed that high expression levels of SLC7A5 in ovarian cancer and inhibition of SLC7A5 can effectively decrease the Kyn content. In addition, the T-cell immune cytotoxic function was decreased in the Kyn-supplemented co-culture system compared with the control group. Thus, targeting the proteins upstream of Kyn metabolism could potentially be an alternative therapeutic treatment for patients with ovarian cancer.

SLC7A5 is an L-type amino acid transporter that functions together with SLC3A2 as a heterodimeric complex at the plasma membrane (37,38). SLC7A5 overexpression has been detected in a number of types of cancer (including breast cancer and lung cancer) (39,40). It has been demonstrated that high SLC7A5 mRNA levels correlate with poor clinical outcomes in a number of types of cancer, such as ovarian cancer and gastric cancer (41,42). Previous retrospective studies have also reported that SLC7A5 overexpression is associated with shorter patient survival in a number of types of cancer, including breast (43), lung (44) and prostate cancers (45). The present study demonstrated that high expression levels of SLC7A5 in ovarian cancer, and inhibition of its activity, could significantly inhibit tumor proliferation, primarily though arrest of the G_2/M phase of the cell cycle. In addition, it was reported that high expression levels of SLC7A5 are present in activated lymphocytes (46,47), which suggested that SLC7A5 expression may also contribute to immunity or immunological responses. However, the underlying mechanism of this process is currently unclear. Kyn is reported to be associated with ligand-activated AHR in transducing tumor immune escape (24). AHR is a transcription factor that regulates the expression of immune checkpoint-related proteins, and thus serves an important role in carcinogenesis and cancer development (48,49). In the present study, inhibition of SLC7A5 transport activity or SLC7A5 expression levels blocked AHR nuclear translocation and decreased PD-L1 expression levels in ovarian cancer cells *in vitro*. The present study additionally examined the *in vivo* biological effects of SLC7A5 expression levels on the enhancement of PD-1 immunotherapy, which suggested that SLC7A5 could potentially serve as a therapeutic target for ovarian cancer immunotherapy.

In conclusion, the present study demonstrated the importance of the SLC7A5-Kyn-AHR-PD-L1 signaling pathway in ovarian cancer cells. The impact of targeting SLC7A5 in ovarian cancer on cell survival and innate immunological response (Fig. 6) provides novel insights into the diagnosis and treatment of ovarian cancer.

Acknowledgements

Not applicable.

Funding

The present work was supported by the Zhejiang Provincial Medicine and Health Science Fund (grant no. 2019RC025), the Natural Science Foundation of Zhejiang Province (grant no. LQ12H16015) and the National Natural Science Foundation of China Grant (grant no. 82003188).

Availability of data and materials

The data generated in the present study may be found in the OMIX (China National Center for Bioinformation/Beijing Institute of Genomics, Chinese Academy of Sciences) database under accession no. OMIX007054 or at the following URL: https://ngdc.cncb.ac.cn/omix/release/OMIX007054.

Authors' contributions

RJ, LG and BJ designed this study. RJ, YS, ZC and LY analyzed the data. RJ performed the experiments with contributions from the DW, CP and JF. RJ wrote the manuscript. RJ and LG confirm the authenticity of all the raw data. All authors have read and approved the final version of the manuscript.

Ethics approval and consent to participate

All patient donors signed written informed consent forms. Ethical approval was obtained from the Ethics Committee of Zhejiang Cancer Hospital (approval no. IRB-2021-315; Hangzhou, China). Patient-derived cells were obtained from an patient with ovarian cancer during surgery in Zhejiang Cancer Hospital who provided signed informed consent forms, as approved by the Ethics Committee of the Zhejiang Cancer Hospital [approval no. (2015)-1-7; Hangzhou, China]. This study was conducted in accordance with the Declaration of Helsinki. All animal experiments were conducted in accordance with the National Institutes of Health Guide for the Care and Use of Laboratory Animals and were approved by the Zhejiang Cancer Hospital Laboratory Animal Ethics Committee (approval no. 2021-05-003; Hangzhou, China).

Patient consent for publication

Not applicable.

Competing interests

The authors declare that they have no competing interests.

References

1. Oza AM, Pierce A, Lau A, Kurian N, Parr G, Lao-Sirieix SH, Ah-See MLW, Dean E and Loembé B: DUETTE: A randomized phase II study to assess a second maintenance treatment with olaparib (ola) or ola+ceralasertib (cer), in patients (pts) with platinum-sensitive relapsed (PSR) epithelial ovarian cancer who have previously received PARP inhibitor maintenance treatment (NCT04239014). J Clin Oncol 38 (15 Suppl): TPS6104, 2020.
2. Ruibin J, Bo J, Danying W, Jianguo F and Linhui G: Cardamonin induces G2/M phase arrest and apoptosis through inhibition of NF-κB and mTOR pathways in ovarian cancer. Aging (Albany NY) 12: 25730-25743, 2020.
3. Ruibin J, Bo J, Danying W, Chihong Z, Jianguo F and Linhui G: Therapy effects of wogonin on ovarian cancer cells. Biomed Res Int 2017: 9381513, 2017.
4. De La Franier B and Thompson M: Early stage detection and screening of ovarian cancer: A research opportunity and significant challenge for biosensor technology. Biosens Bioelectron 135: 71-81, 2019.
5. Jiang R, Chen Z, Ni M, Li X, Ying H, Fen J, Wan D, Peng C, Zhou W and Gu L: A traditional gynecological medicine inhibits ovarian cancer progression and eliminates cancer stem cells via the LRPPRC-OXPHOS axis. J Transl Med 21: 504, 2023.
6. Cai Y, Wang Z, Guo S, Lin C, Yao H, Yang Q, Wang Y, Yu X, He X, Sun W, *et al*: Detection, mechanisms, and therapeutic implications of oncometabolites. Trends Endocrinol Metab 34: 849-861, 2023.
7. Yang K, Wang X, Song C, He Z, Wang R, Xu Y, Jiang G, Wan Y, Mei J and Mao W: The role of lipid metabolic reprogramming in tumor microenvironment. Theranostics 13: 1774-1808, 2023.
8. Wang Z, Wu X, Chen HN and Wang K: Amino acid metabolic reprogramming in tumor metastatic colonization. Front Oncol 13: 1123192, 2023.
9. Zheng Y, Yao Y, Ge T, Ge S, Jia R, Song X and Zhuang A: Amino acid metabolism reprogramming: Shedding new light on T cell anti-tumor immunity. J Exp Clin Cancer Res 42: 291, 2023.
10. Dang CV: Links between metabolism and cancer. Genes Dev 26: 877-890, 2012.
11. Daye D and Wellen KE: Metabolic reprogramming in cancer: Unraveling the role of glutamine in tumorigenesis. Semin Cell Dev Biol 23: 362-369, 2012.
12. Xiao Z, Dai Z and Locasale JW: Metabolic landscape of the tumor microenvironment at single cell resolution. Nat Commun 10: 3763, 2019.
13. Vander Heiden MG, Cantley LC and Thompson CB: Understanding the Warburg effect: The metabolic requirements of cell proliferation. Science 324: 1029-1033, 2009.
14. Liberti MV and Locasale JW: The Warburg effect: How does it benefit cancer cells? Trends Biochem Sci 41: 211-218, 2016.
15. Pavlova NN and Thompson CB: The emerging hallmarks of cancer metabolism. Cell Metab 23: 27-47, 2016.
16. Friedrich M, Sankowski R, Bunse L, Kilian M, Green E, Guevara CR, Pusch S, Poschet G, Sanghvi K, Hahn M, *et al*: Tryptophan metabolism drives dynamic immunosuppressive myeloid states in IDH-mutant gliomas. Nat Cancer 2: 723-740, 2021.
17. Chen W, Wen L, Bao Y, Tang Z, Zhao J, Zhang X, Wei T, Zhang J, Ma T, Zhang Q, *et al*: Gut flora disequilibrium promotes the initiation of liver cancer by modulating tryptophan metabolism and up-regulating SREBP2. Proc Natl Acad Sci a USA 119: e2203894119, 2022.
18. Venancio PA, Consolaro MEL, Derchain SF, Boccardo E, Villa LL, Maria-Engler SS, Campa A and Discacciati MG: Indoleamine 2,3-dioxygenase and tryptophan 2,3-dioxygenase expression in HPV infection, SILs, and cervical cancer. Cancer Cytopathol 127: 586-597, 2019.
19. Ala M: Tryptophan metabolites modulate inflammatory bowel disease and colorectal cancer by affecting immune system. Int Rev Immunol 41: 326-345, 2022.
20. Austin CJD and Rendina LM: Targeting key dioxygenases in tryptophan-kynurenine metabolism for immunomodulation and cancer chemotherapy. Drug Discov Today 20: 609-617, 2015.
21. Lee SH, Mahendran R, Tham SM, Thamboo TP, Chionh BJ, Lim YX, Tsang WC, Wu QH, Chia JY, Tay MHW, *et al*: Tryptophan-kynurenine ratio as a biomarker of bladder cancer. BJU Int 127: 445-453, 2021.
22. Greene LI, Bruno TC, Christenson JL, D'Alessandro A, Culp-Hill R, Torkko K, Borges VF, Slansky JE and Richer JK: A role for tryptophan-2,3-dioxygenase in CD8 T-cell suppression and evidence of tryptophan catabolism in breast cancer patient plasma. Mol Cancer Res 17: 131-139, 2019.
23. Qin R, Zhao C, Wang CJ, Xu W, Zhao JY, Lin Y, Yuan YY, Lin PC, Li Y, Zhao S and Huang Y: Tryptophan potentiates $CD8^+$ T cells against cancer cells by TRIP12 tryptophanylation and surface PD-1 downregulation. J Immunother Cancer 9: e002840, 2021.
24. Cheong JE and Sun L: Targeting the IDO1/TDO2-KYN-AhR pathway for cancer immunotherapy-challenges and opportunities. Trends Pharmacol Sci 39: 307-325, 2018.
25. Nambirajan A, Malgulwar PB, Sharma A, Boorgula MT, Doddamani R, Singh M, Suri V, Sarkar C and Sharma MC: Clinicopathological evaluation of PD-L1 expression and cytotoxic T-lymphocyte infiltrates across intracranial molecular subgroups of ependymomas: Are these tumors potential candidates for immune check-point blockade? Brain Tumor Pathol 36: 152-161, 2019.

26. Wu B, Song M, Dong Q, Xiang G, Li J, Ma X and Wei F: UBR5 promotes tumor immune evasion through enhancing IFN-γ-induced PDL1 transcription in triple negative breast cancer. Theranostics 12: 5086-5102, 2022.
27. Chen Z, Gao Y, Huang X, Yao Y, Chen K, Zeng S and Mao W: Tissue-based metabolomics reveals metabolic biomarkers and potential therapeutic targets for esophageal squamous cell carcinoma. J Pharm Biomed Anal 197: 113937, 2021.
28. Livak KJ and Schmittgen TD: Analysis of relative gene expression data using real-time quantitative PCR and the 2(-Delta Delta C(T)) method. Methods 25: 402-408, 2001.
29. Gostner JM, Obermayr E, Braicu IE, Concin N, Mahner S, Vanderstichele A, Sehouli J, Vergote I, Fuchs D and Zeillinger R: Immunobiochemical pathways of neopterin formation and tryptophan breakdown via indoleamine 2,3-dioxygenase correlate with circulating tumor cells in ovarian cancer patients-A study of the OVCAD consortium. Gynecol Oncol 149: 371-380, 2018.
30. Xia L, Oyang L, Lin J, Tan S, Han Y, Wu N, Yi P, Tang L, Pan Q, Rao S, *et al*: The cancer metabolic reprogramming and immune response. Mol Cancer 20: 28, 2021.
31. Platten M, Wick W and Van den Eynde BJ: Tryptophan catabolism in cancer: Beyond IDO and tryptophan depletion. Cancer Res 72: 5435-5440, 2012.
32. Mor A, Tankiewicz-Kwedlo A and Pawlak D: Kynurenines as a novel target for the treatment of malignancies. Pharmaceuticals (Basel) 14: 606, 2021.
33. Garcia R and Conacci Sorrell M: Investigating the tryptophan-metabolizing enzyme AFMID (arylformamidase) in colon cancer. FASEB J 36, 2022.
34. Van den Eynde BJ, van Baren N and Baurain JF: Is there a clinical future for IDO1 inhibitors after the failure of epacadostat in melanoma? Ann Rev Cancer Biol 4: 241-256, 2020.
35. Chen S, Tan J and Zhang A: The ups, downs and new trends of IDO1 inhibitors. Bioorg Chem 110: 104815, 2021.
36. Kim C, Lee NK, Kim JS, Kim WR, Kim DH, Kim DJ, Oh JS, Chang SK, Kim JW and Chon HJ: An oral dual inhibitor of IDO and TDO enhances anti-cancer immunity and synergizes with immune checkpoint blockade. Ann Oncol 29: viii416, 2018.
37. Yanagida O, Kanai Y, Chairoungdua A, Kim DK, Segawa H, Nii T, Cha SH, Matsuo H, Fukushima J, Fukasawa Y, *et al*: Human L-type amino acid transporter 1 (LAT1): Characterization of function and expression in tumor cell lines. Biochim Biophys Acta 1514: 291-302, 2001.
38. Yan R, Zhao X, Lei J and Zhou Q: Structure of the human LAT1-4F2hc heteromeric amino acid transporter complex. Nature 568: 127-130, 2019.
39. Zhu Q, Wang J, Shi Y, Zha X and Wang S: Bioinformatics prediction and in vivo verification identify SLC7A5 as immune infiltration related biomarker in breast cancer. Cancer Manag Res 14: 2545-2559, 2022.
40. Liu Y, Ma G, Liu J, Zheng H, Huang G, Song Q, Pang Z and Du J: SLC7A5 is a lung adenocarcinoma-specific prognostic biomarker and participates in forming immunosuppressive tumor microenvironment. Heliyon 8: e10866, 2022.
41. Saito Y and Soga T: Amino acid transporters as emerging therapeutic targets in cancer. Cancer Sci 112: 2958-2965, 2021.
42. Ding K, Tan S, Huang X, Wang X, Li X, Fan R, Zhu Y, Lobie PE, Wang W and Wu Z: GSE1 predicts poor survival outcome in gastric cancer patients by SLC7A5 enhancement of tumor growth and metastasis. J Biol Chem 293: 3949-3964, 2018.
43. Shennan DB and Thomson J: Inhibition of system L (LAT1/CD98hc) reduces the growth of cultured human breast cancer cells. Oncol Rep 20: 885-889, 2008.
44. Rajasinghe LD, Hutchings M and Gupta SV: Delta-tocotrienol modulates glutamine dependence by inhibiting ASCT2 and LAT1 transporters in non-small cell lung cancer (NSCLC) cells: A metabolomic approach. Metabolites 9: 50, 2019.
45. Xu M, Sakamoto S, Matsushima J, Kimura T, Ueda T, Mizokami A, Kanai Y and Ichikawa T: Up-regulation of LAT1 during Antiandrogen therapy contributes to progression in prostate cancer cells. J Urol 195: 1588-1597, 2016.
46. Hayashi K, Kaminuma O, Nishimura T, Saeki M, Matsuoka K, Hiroi T, Jutabha P, Iwata Y, Sugiura K, Owada T, *et al*: LAT1-specific inhibitor is effective against T cell-mediated allergic skin inflammation. Allergy 75: 463-467, 2020.
47. Cibrian D, Saiz ML, de la Fuente H, Sánchez-Díaz R, Moreno-Gonzalo O, Jorge I, Ferrarini A, Vázquez J, Punzón C, Fresno M, *et al*: CD69 controls the uptake of L-tryptophan through LAT1-CD98 and AhR-dependent secretion of IL-22 in psoriasis. Nat Immunol 17: 985-996, 2016.
48. Budhwar S, Bahl C, Sharma S, Singh N and Behera D: Role of sequence variations in AhR gene towards modulating smoking induced lung cancer susceptibility in north indian population: A multiple interaction analysis. Curr Genomics 19: 313-326, 2018.
49. Helou DG, Shafiei-Jahani P, Hurrell BP, Painter JD, Quach C, Howard E and Akbari O: LAIR-1 acts as an immune checkpoint on activated ILC2s and regulates the induction of airway hyperreactivity. J Allergy Clin Immunol 149: 223-236. e6, 2022.